NANO LETTERS

Letter

pubs.acs.org/NanoLett

A Nanostructured Electrochromic Supercapacitor

Di Wei,*[,†,§] Maik R. J. Scherer,[‡,§] Chris Bower,[†] Piers Andrew,[†] Tapani Ryhänen,[†] and Ullrich Steiner*[,‡]

[†]Nokia Research Center, Broers Building, J. J. Thomson Avenue, CB3 0FA, Cambridge, United Kingdom

[‡]Department of Physics, University of Cambridge, J. J. Thomson Avenue, CB3 0HE, Cambridge, United Kingdom

Supporting Information

ABSTRACT: We report the first successful application of an ordered bicontinuous double-gyroid vanadium pentoxide network in an electrochromic supercapacitor. The freestanding vanadia network was fabricated by electrodeposition into a voided block copolymer template that had self-assembled into the double-gyroid morphology. The highly ordered structure with 11.0 nm wide struts and a high specific surface to bulk volume ratio of 161.4 μm^{-1} is ideal for fast and efficient lithium ion intercalation/extraction and faradaic surface reactions, which are essential for high energy and high power density electrochemical energy storage devices. Supercapacitors made from such gyroid-structured vanadia electrodes exhibit a high specific capacitance of 155 F g^{-1} and show a strong electrochromic color change from green/gray to yellow, indicating the capacitor's charge condition. The nanostructuring approach and utilizing an electrode material that has intrinsic electrochemical color-change properties are concepts that can be readily extended to other electrochromic intercalation compounds.

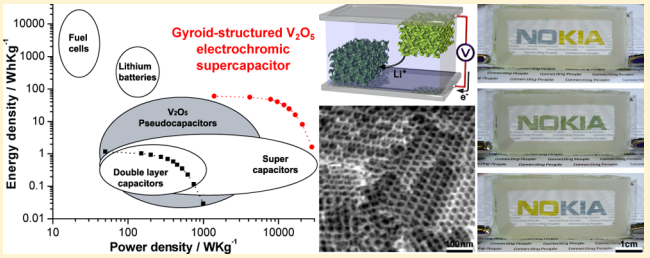

KEYWORDS: *Electrochromic supercapacitor, vanadium pentoxide, copolymer self-assembly, double-gyroid, nanostructured intercalation compound*

Growing interest in electric vehicles allied with the ubiquity of increasingly capable mobile devices create a seemingly insatiable demand for electrochemical energy storage with higher power and energy densities. These two requirements, unfortunately, cannot be met by current energy storage devices. While lithium batteries provide high energy density storage, they deliver only limited power upon discharge. Supercapacitors, a form of electrochemical energy storage device with short charging times, have the ability to deliver significantly more power but store less energy. In this work, we report the manufacture of supercapacitors employing nanostructured transition metal oxide electrodes. Vanadium pentoxide (V_2O_5) forming a bicontinuous gyroid structure on the 10 nm scale was used to fabricate supercapacitors, yielding devices with a promising combination of high power and energy densities. Furthermore, the electrochromic response of these electrodes allowed the visualization of the device charge state as the degree of color saturation indicates the energy storage level of the device.

There are two types of supercapacitors, differentiated by their charge storage mechanism. In the electrochemical double layer capacitor (EDLC), charge is stored electrostatically by the reversible and very rapid adsorption and desorption of ions on/from high-surface-area materials, for example, activated carbon. The charges accumulate in the electrical double layer at the electrode/electrolyte interface. A major limitation of traditional EDLCs is their low energy density, which accounts for the increased interest in the use of redox materials for electrochemical capacitors with energy densities that are increased by more than 1 order of magnitude. In the second type of supercapacitor, known as a pseudocapacitor, kinetically facile faradaic reactions occur at the electrode surface and electrons are transferred to or from the valence bands of the redox cathode or anode reagent.[1] Capacitive contributions arise from charge-transfer processes with surface atoms as well as near-surface ion intercalation, referred to as redox and intercalation pseudocapacitance, respectively. The definition of pseudocapacitance requires that both these faradaic processes are kinetically facile and not diffusion controlled on the time scale of interest.[2] Such surface faradaic reactions are slower than ionic adsorption/desorption, resulting in slower charge/discharge rates compared to EDLCs, but faster than in batteries, where faradaic reactions take place in the bulk of the electrode, rather than at the electrode surface.[3] However, diffusion controlled ion insertion and double layer formation might also contribute to the total charge stored in pseudocapacitors.[4]

The specific energy of lithium ion batteries is typically of the order of 100−1000 Wh kg^{-1}, but the specific power is only of the order of 0.1 kW kg^{-1}. The typical specific energy and power of EDLCs are of the order of 1 Wh kg^{-1} and 1 kW kg^{-1}, respectively. These specific values are not high enough to replace batteries in many applications. Nanostructured

Received: November 30, 2011
Revised: February 6, 2012
Published: March 5, 2012

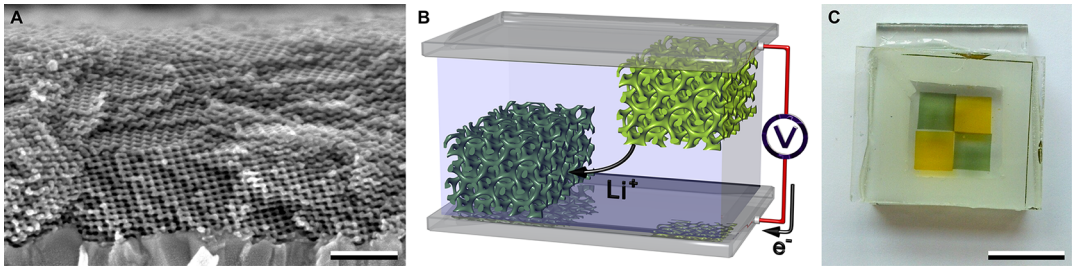

Figure 1. Nanostructure and design of electrochromic supercapacitors. (A) Cross-sectional scanning electron micrograph of a mesoporous V_2O_5 double-gyroid film on a FTO substrate (scale bar: 200 nm). (B) Schematic illustration of the supercapacitor design based on two laterally offset double-gyroid structured electrodes. (C) Photograph of a fully transparent electrochromic supercapacitor consisting of an oxidized yellow top electrode, a laterally offset green/gray bottom electrode in the reduced state, and a thermoplastic gasket spacer (scale bar: 1 cm).

transition metal oxide architectures have been developed to allow both redox and intercalation pseudocapacitance. This approach has the potential to simultaneously optimize the energy and power densities in a single material. One way to increase pseudocapacitance is to increase electrode surface area.

V_2O_5 aerogels can act as high rate, high capacity hosts for lithium, because they have a very high surface area and the diffusion distance that must be penetrated by lithium is very short.[5] Amorphous V_2O_5 in a nanoporous alumina template showed a high specific capacitance of 900 F g^{-1} in 1 M KCl electrolyte.[6] Promising capacitive behavior was observed for hydrous vanadium oxide with specific capacitance reaching 737 F g^{-1} in 12 M LiCl for a potential window between −0.2 and 0.8 V.[7] Ideal supercapacitor behavior with large specific capacitance (~350 F kg^{-1}) of amorphous $V_2O_5{\cdot}nH_2O$ in aqueous solution containing KCl with optimized pH has been reported.[8] However, the application of water in supercapacitors limits their operation temperature as well as the electrochemical window. Electrospun V_2O_5 nanofibers as supercapacitor electrodes showed a promising energy density of 5 Wh kg^{-1}.[9] V_2O_5 has also been applied in lithium batteries with a discharge−charge efficiency up to 97.2% in the potential range from 2 to 4 V.[10] High-performance supercapacitors based on intertwined carbon nanotube/V_2O_5 nanowire composites exhibit specific energy capacity of 40 Wh kg^{-1} and a power density of 210 W kg^{-1}.[11] Binder-free flexible supercapacitors containing vanadium oxide nanowires and carbon nanotubes showed further improvement in power density (5.26 kW kg^{-1}) and energy density (46.3 Wh kg^{-1}).[12] High-intercalation rates of V_2O_5 gel/carbon composites in supercapacitors were also reported with a specific energy density of 20 Wh kg^{-1}.[13] Pseudocapacitors made from V_2O_5-coated self-standing carbon-nanofiber paper achieved a specific capacitance per mass of vanadia of 1308 F g^{-1} in a 2 M KCl electrolyte, although this high value decreases to 214 F g^{-1} when considering the total mass of the composite electrode.[14] Three-dimensional bicontinuous ultrafast-charge and discharge bulk battery electrodes made by electrodeposition through colloidal templates have been reported.[15] Similarly, filigree metal oxide architectures can be achieved with templates, using polymer building blocks which self-assemble into a periodic continuous network and the subsequent removal of one of the network components to generate a porous matrix.

Here, we demonstrate that enhanced pseudocapacitance can be achieved using a self-supporting double-gyroid (DG) structure of V_2O_5. The interconnected bicontinuous DG morphology with $Ia\bar{3}d$ symmetry shows high structural stability and offers an extremely high active surface area, which is easily accessible by an electrolyte, due to its interconnected porous network and homogeneous pore diameter. The enhanced electrochromic performance of such nanostructured vanadia was demonstrated previously.[16] The fast intercalation of lithium ions in the DG structure enables the visualization of energy density by change in color, a concept that applies to the charge state of the pseudocapacitors presented here.

The fabrication route, material characterization, and electrochromic properties of DG V_2O_5 films have been reported in detail elsewhere.[16] Briefly, voided styrenic DG templates on conducting fluorine tin oxide (FTO) coated glass were prepared by temperature annealing spin-coated films of poly(4-fluorostyrene-*r*-styrene)-*b*-poly(D,L-lactide) at 175 °C for 20 min and subsequent removal of the polylactide minority phase (see Supporting Information, Figure S1). The diblock copolymer used in this study had a molecular weight of 23.8 kg mol^{-1} and contained 37.9% vol polylactide. Templated and nontemplated anodic deposition of V_2O_5 films was performed at a constant potential of 1.5 V versus Ag/AgCl for 120 s from a 1:1 mixture of deionized water and ethanol, containing 1 M of $VOSO_4{\cdot}xH_2O$. The deposition rate of nontemplated films was significantly faster. After the removal of the styrenic template by dissolution in toluene and temperature annealing at 275 °C in air for 2 h, the vanadia films were ready for further characterization. Scanning electron micrographs of the mesoporous, highly periodic DG V_2O_5 replica with a cubic unit cell size of 41.5 ± 1 nm, a corresponding strut diameter of 11.0 ± 0.3 nm, and a specific surface to bulk volume ratio of 161.4 m^{-1} are presented in Figure 1A and Supporting Information Figure S2.[16] The density of electrodeposited nontemplated vanadia is assumed to be ~2.87 g cm^{-3}, thus the average density of DG structured vanadia with a volume fraction of 37.9% is ~1.09 g cm^{-3}, illustrating the porous nature of the DG structure.[17]

The electrochemical behavior of the V_2O_5 material was investigated using a three-electrode electrochemical cell in which lithium foils were used as both the counter and reference electrodes under a protective argon atmosphere. The V_2O_5 samples formed the working electrode and two types of V_2O_5 structures were studied, a DG nanostructure and an unstructured compact layer. Cyclic voltammetry was used to investigate the Li insertion/extraction behavior in 1 M $LiClO_4$ propylene carbonate solution with a scan rate of 1 mV s^{-1}.

Figure 2 shows typical cyclic voltammograms (CVs) of V_2O_5 in the potential range of 2−4 V (vs Li/Li^+). Over this potential range, the V_2O_5 electrodes are expected to undergo reversible

dx.doi.org/10.1021/nl2042112 | *Nano Lett.* 2012, 12, 1857−1862

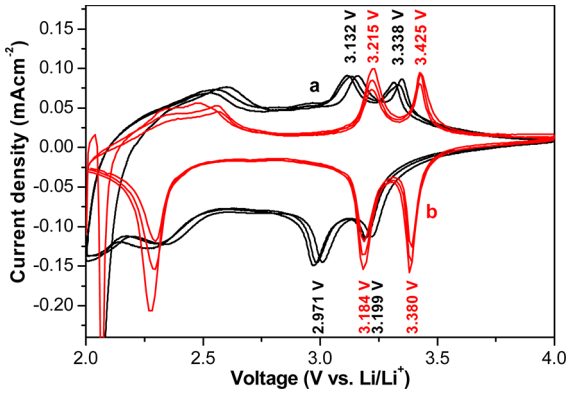

Figure 2. Cyclic voltammogram of V_2O_5, measured in 1 M $LiClO_4$ propylene carbonate solution for a nontemplated V_2O_5 layer (a) and double-gyroid structured V_2O_5 (b).

lithium ion insertion, which is accompanied by color changes and occurs in two consecutive stages[18,19]

$$V_2O_5 + 0.5Li^+ + 0.5e^- \leftrightarrow Li_{0.5}V_2O_5 \quad (1)$$

$$Li_{0.5}V_2O_5 + 0.5Li^+ + 0.5e^- \leftrightarrow LiV_2O_5 \quad (2)$$

The above processes are reflected in the slow scanning rate (1 mV s^{-1}) CV of the nontemplated V_2O_5 electrodes as two well-resolved sets of peaks. For the DG nanostructured V_2O_5 electrodes (Figure 2b), only a fraction of the V^{5+} ions are reduced to V^{4+} ions in the first reduction peak at about 3.4 V. This reduction changes the color of the material from yellow to green. The remaining V^{5+} ions are reduced to V^{4+} in the second peak at 3.2 V. The reverse reactions give rise to the two corresponding oxidation peaks in the reverse scan. Two phases of $Li_xV_2O_5$ are typically formed in this electrochemical reaction. The binary phase diagram of V_2O_5–$Li_xV_2O_5$ indicates that the peaks at 3.2 and 3.4 V correspond to the phase transformation from α-V_2O_5 to ε-V_2O_5 and from ε-V_2O_5 to δ-V_2O_5, respectively.[20] For the DG nanostructured V_2O_5, the color changes from green/gray to yellow when the voltage is above 3.5 V.

The two sample types differ in the location and separation distance of the CV peaks. For the same experimental conditions, the anodic voltage peaks lie at ~3.4 and ~3.2 V for DG structured V_2O_5, more than 200 mV higher than the nontemplated layer with ~3.2 and ~3.0 V, respectively. The average voltage difference between the cathodic and the corresponding anodic double-peak of the redox reactions in Figure 2 decreases from 150 mV for the nontemplated layer to 38 mV for the DG material. A further reversible redox process is observed in the 2–2.8 V potential range, where a second lithiation step takes place. This deep lithiation occurring at 2 V changes the color from green to blue and may cause structural change. These structural changes have no detrimental effect on the reversible lithium insertion at capacities corresponding to the uptake of 2 Li atoms per V_2O_5 in the 2–4 V potential range.[19]

The V_2O_5 materials were then used to fabricate supercapacitors. A highly conducting room temperature ionic liquid (RTIL), triethylsulfonium bis(trifluoromethylsulfonyl) imide ([SET3][TFSI]), was chosen as electrolyte. RTILs are molten salts with a melting point close to or below room temperature. They are composed of bulky organic cations and smaller anions that only loosely associate. Their good solvation properties, high conductivity, nonvolatility, low toxicity, and good electrochemical stability make RTILs suitable for many electrochemical applications. Nonflammable RTIL gels have been used as electrolyte in supercapacitors, enabling flexibility, safe operation, and a large electrochemical window (i.e., the electrochemical potential range over which the electrolyte is neither reduced nor oxidized at the electrodes).[21] Unlike organic solvents, the high boiling point of RTILs makes the encapsulation of the device easier and avoids electrolyte evaporation during testing, thereby further enhancing the cyclability of the device. Lithium bis(trifluoromethylsulfonyl) imide (LiTFSI) was used as lithium salt since it has the same anion as the RTIL. The supercapacitor was assembled with a pair of electrodes made of FTO coated glass sheets each coated with approximately 1 μm thick DG nanostructured V_2O_5. Electrochemical testing was performed using supercapacitor devices prepared by sandwiching a precut thermoplastic gasket as spacer between laterally offset electrodes obviating the need for a separator and enabling the observation of color change of both electrodes as shown in Figure 1B,C and Figure 5. After assembly the electrolyte was infiltrated using a syringe and the cell was sealed with epoxy glue.

The electrochemical properties of such supercapacitors with templated and nontemplated electrodes were studied by cyclic voltammetry at a sweep rate of 50 mV s^{-1} for voltage sweeps between −1 and 1 V and from −0.5 to 0.5 V. In the potential range from −0.5 to 0.5 V, both V_2O_5 materials exhibit nearly rectangular CV traces, indicating good capacitive characteristics for the devices. In the −1 to 1 V potential range, supercapacitors with lithium salt containing electrolyte (Figure 3Aa,Ba) showed pseudocapacitive redox peaks. The capacitive current density of the DG V_2O_5 (Figure 3Ba) is much higher compared to the significantly thicker and denser nontemplated V_2O_5 film (Figure 3Aa).

As the structure of electrochemically active materials approaches nanoscale dimensions, pseudocapacitive effects become increasingly important. The dependence of pseudocapacitance on the size of anatase TiO_2 nanocrystals has been established quantitatively.[4] The results showed that for particles smaller than 10 nm in diameter, more than half of the total charge is stored via pseudocapacitive processes. The contribution of faradaic and double-layer capacitances in the response of DG nanostructured V_2O_5 can be estimated by comparing the CV curves of devices that use RTIL electrolyte with and without lithium salt, shown in Figure 3B. Since V_2O_5 does not react with either of the ions of pure RTIL, the lithium-free experiment tests the EDLC response. With lithium salt added, the significant increase in capacitive current and the appearance of peak pairs indicates that redox reactions are taking place. These faradaic processes are kinetically facile and thus considered pseudocapacitive, but phase transitions cannot be excluded. Although it is difficult to distinguish between redox and intercalation pseudocapacitance, the latter is likely to be present in DG bicontinuous materials.

The specific capacitance of a Li-free EDLC-based DG nanostructure is 25.8 F g^{-1}, about 1 order of magnitude larger compared to a nontemplated layer based device of only ~3 F g^{-1}. When adding lithium salt, the specific capacitance for the DG structured V_2O_5 pseudocapacitor raises significantly. Figure 4B shows the cycle stability of the two V_2O_5-based systems containing lithium salt. The gyroid structured materials had an initial specific capacitance of 422 F g^{-1}, which equilibrated to the steady state of 155 F g^{-1} after 10 switching cycles at a high

dx.doi.org/10.1021/nl2042112 | *Nano Lett.* 2012, 12, 1857–1862

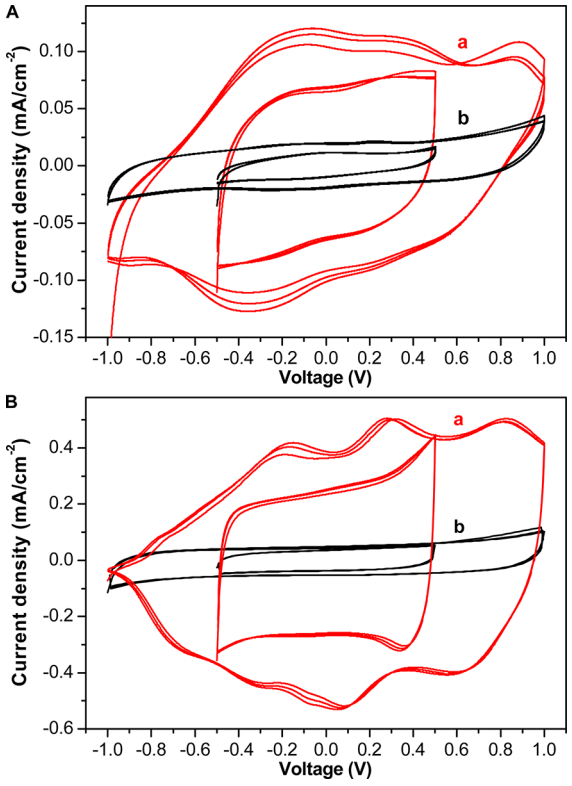

Figure 3. Cyclic voltammograms of supercapacitors made with V_2O_5 electrodes. CV of a nontemplated layer (A) and double-gyroid structured (B) electrode films, where (a) is the CV cycled with an RTIL electrolyte containing lithium salt and (b) is the CV using Li-free RTIL as electrolyte, displaying an electric double layer response. The cycled potential ranges are −0.5 to 0.5 V (inner curves) and −1 to 1 V (outer curves) with a scan rate of 50 mV s^{-1}. Note the widely different ordinate scales.

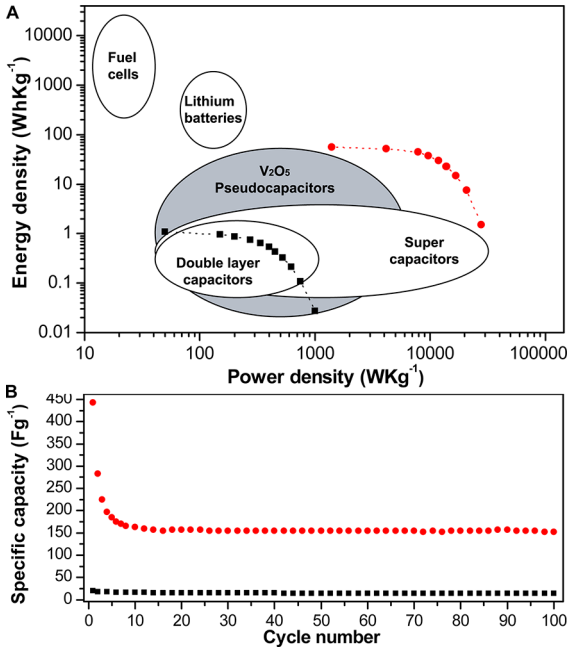

Figure 4. Ragone plot of electrochemical energy storage devices and supercapacitor stability. The pseudocapacitive performance (A) and specific capacitance (B) of double gyroid supercapacitors (●) and nontemplated layer V_2O_5 (■) for a fixed ±4 V potential window are compared (for the corresponding charge−discharge curves see Supporting Information, Figures S3 and S4). The double-gyroid structured pseudocapacitor gave very high initial specific capacitance of 442 F g^{-1} that stabilized at 155 F g^{-1} after 10 cycles at high current density >10 A g^{-1}. In contrast, the specific capacitance of the nontemplated V_2O_5 layer drops from an initial 20 to about 14 F g^{-1}.

current density >10 A g^{-1}. The nontemplated layer material showed a much more gradual variation, dropping from an initial 20 to 14 F g^{-1}. The charge storage ability of supercapacitors is directly linked to the geometric confinement of ions in extremely small pores and the availability of a large surface area. The much higher specific surface area of the DG nanostructured V_2O_5 compared to the nontemplated material therefore partly explains the substantial improvement in capacitive current.

The overall performance of our V_2O_5-based supercapacitors is summarized in the Ragone plot describing the relation between energy density and power density (Figure 4A).[11] The highest obtained energy density of nontemplated vanadia supercapacitors is 1 Wh kg^{-1} at a power density of 50 W kg^{-1} that drops by 50% at a power density of 0.4 kW kg^{-1}. Such low values arise from the limited ion diffusion into the thick nontemplated V_2O_5 electrode, resulting also in a lack of responsiveness of the device. The maximization of the response time in nontemplated layer devices limits the thickness of most pseudocapacitive electrodes to submicrometer values.[2,22,23]

On the other hand, devices made from DG V_2O_5, exhibit energy densities as high as 52 Wh kg^{-1} at power densities above 1 kW kg^{-1}. Even at power densities as high as 16.7 kW kg^{-1}, the best performing device still had an energy density of 13.9 Wh kg^{-1}, placing them among the top performing V_2O_5 devices.[11] The energy density of a supercapacitor is governed by the overall capacitance and the operating voltage. The use of organic electrolytes can increase the operating voltage compared to aqueous electrolytes.[9] RTILs are very promising solvent-free electrolytes that greatly broaden the electrochemical window during device operation, thus enabling high-voltage supercapacitors with enhanced energy densities. Combined with the introduction of interconnected porosity in DG V_2O_5 significantly enhances the electrochemical properties, stemming from a combination of electrolyte access, short Li^+ penetration lengths, good electronic transport, and large surface area of nanostructure enabling Li^+ insertion/extraction.[2] This leads to the observed conjunction of high specific energy and power densities of DG V_2O_5 supercapacitors, with energy densities approaching the lower end of lithium batteries.

Nontemplated V_2O_5 devices have an electrochromic switching time of several minutes and the color change is therefore not sufficiently rapid for observation when charging and discharging the device. The improvement of ion intercalation in the DG V_2O_5 supercapacitor gives rise to rapid color changes and high chromatic contrast (Figures 1C and Figure 5). In situ UV−vis-NIR measurements of the transmissivity of DG V_2O_5 films were carried out during chronopotentiometry with a current density of ±2 mA cm^{-2} and a 20 s polarity switching interval (Figure 6). The anode attained the fully oxidized state, revealing a vivid yellow color, after 20 s when the potential reached 3.5 V, while the cathode exhibited the green/gray reduced state. The optical transmission spectra of the reduced and oxidized states are shown in Figure 6A. The oxidized state showed a strong absorption peak around 425 nm, while the electrode was mainly transparent at wavelengths above 580 nm.

dx.doi.org/10.1021/nl2042112 | *Nano Lett.* 2012, 12, 1857−1862

Figure 5. Photographs of an electrochromic supercapacitor device displaying color change upon charge and discharge. The letters "NO" form the double-gyroid structured top electrode and "KIA" the bottom electrode (scale bar: 1 cm). Both V_2O_5 electrodes have identical area. (A) Discharged green state at 0 V. (B,C) Charged state at ±3.5 V for reverse polarity with green/gray reduced and yellow oxidized electrodes. This device is still fully functional after six months.

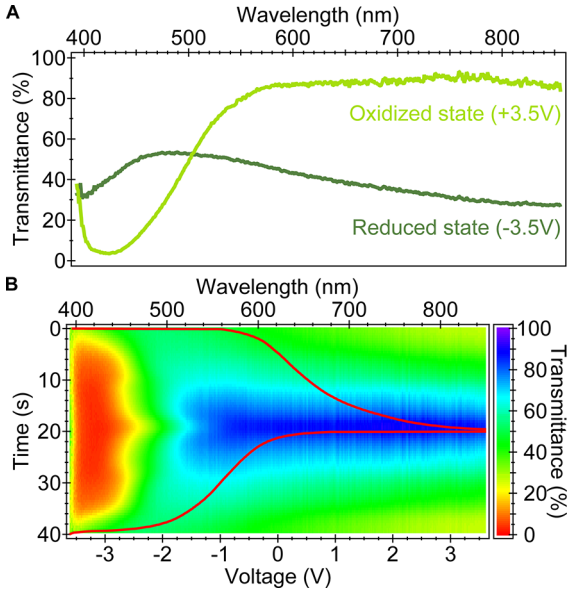

Figure 6. In-situ UV−vis-NIR measurement. (A) Optical transmittance spectra of the fully oxidized and reduced electrodes of the transparent supercapacitor device shown in Figure 1C. (B) Transmittance variation during chronopotentiometry with alternating current polarity (+2 mA cm^{-2} for the initial 20 s and −2 mA cm^{-2} for the remaining time). The red line is the potentiometric response.

The long wavelength transmittance dropped sharply during Li^+ intercalation, while rising at shorter wavelengths. The dynamic optical behavior and the potentiometric response are shown in Figure 6B. The coloration change during oxidation commenced at a potential of −1 V and reached the fully oxidized state at +3.5 V, while the coloration response started at +1 V and ended at −3.5 V during reduction.

Note that Li^+ intercalation into V_2O_5 is intrinsically slow, with a reported diffusion coefficient of the order of 10^{-13} cm^2 s^{-1}.[24] The maximum diffusion length during 100 ms is approximately 5 nm, which corresponds to the radius of the DG struts. The DG nanostructured device therefore responds much faster than the nontemplated layer, while showing more symmetric charge−discharge curves and a much higher energy capacity, overcoming the characteristic slow ion insertion/extraction by diffusion of Li^+ through the V_2O_5 bulk. DG nanostructured V_2O_5 electrodes enable the reversible lithium ion insertion/extraction from RTIL solution in the 0−4 V potential range, corresponding to the insertion of 2 Li ions per V_2O_5 unit.

A commonly observed problem in nanostructured supercapacitors is their initial loss of capacitance during cycling, mainly caused by compaction of the material resulting in a reduced surface area exposed to electrolyte.[22] A performance reduction in V_2O_5 nanowire electrodes may be attributed to a similar mechanism.[11] Some volume expansion occurs upon Li^+ insertion in almost all cathode materials, usually causing an increase in the width of the van der Waals gaps in layered metal oxide systems. In thin films, expansion in the plane of the film is not possible because of substrate pinning, limiting expansion in the direction of the surface normal. With the iso-oriented nature of these materials, in-plane expansion is not required to accommodate the strain of Li^+ insertion because all expansion occurs normal to the substrate. This markedly reduces the stress associated with Li^+ insertion. Although this should be an advantage for all iso-oriented bulk films, it is important to recall that ions enter the van der Waals gaps from the sides of the film. Nanoscale porosity therefore enables the electrolyte to access the interior of the film and exposes the vertical edges of the layers to facile Li^+ insertion. Moreover, previous experiments on structured metal oxide composites have shown that the pore architecture can flex like a nanoscale truss in response to a mechanical load, further facilitating this volume expansion.[25] This unique combination of factors is probably responsible for the fast intercalation pseudocapacitance observed in these materials.

Supercapacitor charge storage offers a number of desirable properties when compared with conventional batteries, including charging within seconds, long-term cycling stability and the ability to deliver up to ten times more power. These features are used not only in high power demanding applications such as power buffers and power saving units, but also in energy recovery. Whereas charge storage through nonfaradaic means is fairly straightforward, a variety of distinct chemical options are available for charge storage through faradaic or redox-type reactions. The results presented here illustrate the benefits of applying a DG nanostructured V_2O_5 in a combined electrochromic and electrochemical energy storage device. The improvement in energy density without compromising power density suggests that this supercapacitor approach may be attractive for a wide range of device applications. This work also validates the nanocomposite approach for the design and fabrication of new types of high energy and high power electrochemical devices. In addition, the improved charge insertion kinetics in the DG structure enables an electrode color change during energy transients. In summary, DG nanostructured V_2O_5 is a promising candidate for high energy and high power density supercapacitors with effective color change during short-time charge and discharge cycles.

■ ASSOCIATED CONTENT

Ⓢ Supporting Information

Scanning electron micrographs of a voided DG template and an annealed DG vanadia film and charge−discharge curves of a plain and DG V_2O_5 supercapacitors. This material is available free of charge via the Internet at http://pubs.acs.org.

■ AUTHOR INFORMATION

Corresponding Author

*E-mail: (D.W.) di.wei@nokia.com; (U.S.) u.steiner@phy.cam.ac.uk.

Author Contributions

§Equal contribution.

Notes

The authors declare no competing financial interest.

■ ACKNOWLEDGMENTS

This work was funded through the Nokia - Cambridge University Strategic Research Alliance in Nanotechnology.

■ REFERENCES

(1) Simon, P.; Gogotsi, Y. *Nat. Mater.* **2008**, *7*, 845−854.
(2) Brezesinski, T.; Wang, J.; Tolbert, S. H.; Dunn, B. *Nat. Mater.* **2010**, *9*, 146−151.
(3) Arico, A. S.; Bruce, P.; Scrosati, B.; Tarascon, J.; van Schalkwijk, W. *Nat. Mater.* **2005**, *4*, 366−377.
(4) Wang, J.; Polleux, J.; Lim, J.; Dunn, B. *J. Phys. Chem. C* **2007**, *111*, 14925−14931.
(5) Parent, M. J.; Passerini, S.; Owens, B. B.; Smyrl, W. H. *J. Electrochem. Soc.* **1999**, *146*, 1346−1350.
(6) Jeon, H.; Jeong, B.; Lee, J. K.; Kim, H. S.; Lee, S.; Lee, J. *Electrochem. Solid-State Lett.* **2010**, *13*, A25−A28.
(7) Li, J.; Chang, K.; Hu, C. *Electrochem. Commun.* **2010**, *12*, 1800−1803.
(8) Lee, H. Y.; Goodenough, J. *J. Solid State Chem.* **1999**, *148*, 81−84.
(9) Wee, G.; Soh, H. Z.; Cheah, Y. L.; Mhaisalkar, S. G.; Srinivasan, M. *J. Mater. Chem.* **2010**, *20*, 6720−6725.
(10) Cao, A.; Hu, J.; Liang, H.; Wan, L. *Angew. Chem., Int. Ed.* **2005**, *44*, 4391−4395.
(11) Chen, Z.; Augustyn, V.; Wen, J.; Zhang, Y.; Shen, M.; Dunn, B.; Lu, Y. *Adv. Mater.* **2011**, *23*, 791−795.
(12) Perera, S. D.; Patel, B.; Nijem, N.; Roodenko, K.; Seitz, O.; Ferraris, J. P.; Chabal, Y. J.; Balkus, K. J. Jr. *Adv. Energy Mater.* **2011**, *1*, 936−945.
(13) Kudo, T.; Ikeda, Y.; Watanabe, T.; Hibino, M.; Miyayama, M.; Abe, H.; Kajita, K. *Solid State Ionics* **2002**, *152*−*153*, 833−841.
(14) Ghosh, A.; Ra, E. J.; Jin, M.; Jeong, H.; Kim, T. H.; Biswas, C.; Lee, Y. H. *Adv. Funct. Mater.* **2011**, *21*, 2541−2547.
(15) Zhang, H.; Yu, X.; Braun, P. V. *Nat. Nanotechnol.* **2011**, *6*, 277−281.
(16) Scherer, M. R. J.; Li, L.; Cunha, P. M. S.; Scherman, O. A.; Steiner, U. *Adv. Mater.* **2012**, *24*, 1217−1221.
(17) Wang, Y.; Takahashi, K.; Lee, K. H.; Cao, G. Z. *Adv. Funct. Mater.* **2006**, *16*, 1133−1144.
(18) Lu, Z.; Levi, M.; Salitra, G.; Gofer, Y.; Levi, E.; Aurbach, D. *J. Electroanal. Chem.* **2000**, *491*, 211−221.
(19) Odani, A.; Pol, V. G.; Pol, S. V.; Koltypin, M.; Gedanken, A.; Aurbach, D. *Adv. Mater.* **2006**, *18*, 1431−1436.
(20) Murphy, D.; Christian, P.; DiSalvo, F.; Waszczak, J. *Inorg. Chem.* **1979**, *18*, 2800−2803.
(21) Wei, D.; Ng, T. W. *Electrochem. Commun.* **2009**, *11*, 1996−1999.
(22) Toupin, M.; Brousse, T.; Bélanger, D. *Chem. Mater.* **2002**, *14*, 3946−3952.
(23) Lee, S. W.; Yabuuchi, N.; Gallant, B. M.; Chen, S.; Kim, B.; Hammond, P. T.; Shao-Horn, Y. *Nat. Nanotechnol.* **2010**, *5*, 531−537.
(24) Passerini, S.; Ressler, J.; Le, D.; Owens, B.; Smyrl, W. *Electrochim. Acta* **1999**, *44*, 2209−2217.
(25) Kirsch, B. L.; Chen, X.; Richman, E. K.; Gupta, V.; Tolbert, S. H. *Adv. Funct. Mater.* **2005**, *15*, 1319−1327.